Improved Reconstruction of 4D-MR Images by Motion Predictions*

Christine Tanner, Golnoosh Samei, and Gábor Székely

Computer Vision Laboratory, ETH Zurich,
Sternwartstrasse 7, 8092 Zurich, Switzerland
tannerch@vision.ee.ethz.ch

Abstract. The reconstruction of 4D images from 2D navigator and data slices requires sufficient observations per motion state to avoid blurred images and motion artifacts between slices. Especially images from rare motion states, like deep inhalations during free-breathing, suffer from too few observations.

To address this problem, we propose to actively generate more suitable images instead of only selecting from the available images. The method is based on learning the relationship between navigator and data-slice motion by linear regression after dimensionality reduction. This can then be used to predict new data slices for a given navigator by warping existing data slices by their predicted displacement field. The method was evaluated for 4D-MRIs of the liver under free-breathing, where sliding boundaries pose an additional challenge for image registration.

Leave-one-out tests for five short sequences of ten volunteers showed that the proposed prediction method improved on average the residual mean (95%) motion between the ground truth and predicted data slice from 0.9mm (1.9mm) to 0.8mm (1.6mm) in comparison to the best selection method. The approach was particularly suited for unusual motion states, where the mean error was reduced by 40% (2.2mm vs. 1.3mm).

1 Introduction

Minimal invasive radiation therapies for the abdomen during free-breathing require guidance for keeping the beam on the moving target. For proton and focused ultrasound therapies, the position of other structures, like bones or vessels, passed through by the beam are also of great importance for accurate calculation of the Bragg Peak, and avoidance of hot and cold spots. Real-time observation and tracking of all structures of interest during therapy is currently not possible. Motion models, which predict the motion of the remaining structures from partial observations have been proposed [1, 2]. For capturing respiratory irregularities, these rely on learning the motion patterns from 4D-MRIs, which allow in comparison to 4D-CTs, for long term observations.

* We acknowledge funding from the EU's Seventh Framework Program (FP7/2007-2013) under grant agreement n^o 270186 (FUSIMO) and n^o 611889 (TRANSFUSIMO). We thank Prof. S. Kozerke and Dr. J. Schmidt (Institute for Biomedical Engineering, University and ETH, Zurich) for their help with the MRI acquisitions.

P. Golland et al. (Eds.): MICCAI 2014, Part I, LNCS 8673, pp. 146–153, 2014.

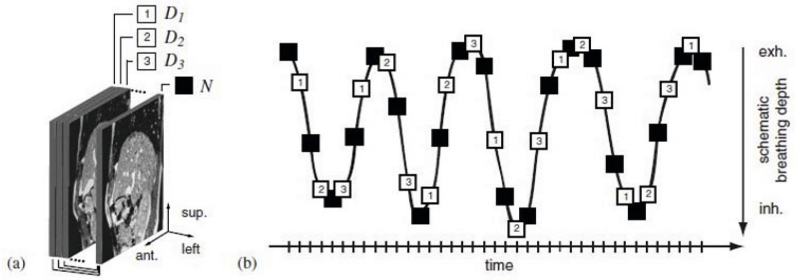

Fig. 1. Illustration of MR sequence with alternating navigator (N) and data slices (D_1,...,D_3). (Courtesy von Siebenthal [3])

4D-MRIs can be created by an interleaved acquisition of 2D navigator and data slices and retrospective sorting [3], as illustrated in Fig. 1. Per data slice, a whole 3D image was created by stacking data slices, which are enclosed by a similar navigator pair as the current one. Similarity was measured by the difference in displacements to a reference navigator slice [3] or by the difference in intensities of the navigators after manifold embedding [4]. To improve SNR of the reconstruction, the mean of the T most similar data slices was employed. 2D navigator-free 4D-MRI reconstruction methods have been proposed, relying for example on external breathing signals [5] or the consistency between neighbouring data slices after manifold embedding [6]. However, we focus here on the 2D navigator-based 4D-MRI liver reconstructions, as the additional information from continuously observing the liver motion at the same position has the potential to provide superior reconstructions and allows for quantitative evaluation.

Currently 4D-MRI reconstructions are based on selecting the most similar images. For unusual motion states, like large inhalations, this leads to blurry images and motion artifacts between slices since the most similar images are quite different. The problem is emphasised for reconstructions from shorter sequences, as fewer motion states are available. In this work, we propose to actively create more similar images by learning the relationship between navigator and data-slice motion, predict for a given navigator motion the data-slice motion and then use this predicted motion to warp the data slice to a more similar position. Additionally, this was compared to using navigator intensities instead of motion.

Mean images have previously been sharpened by image registration in the field of superresolution [7, 8] and atlas creation e.g. [9–11]. In the former application, SNR and image resolution is generally improved for an existing image by registering images of additional observations to it. This task is much simpler than our problem due to the existence of a reference image. Early works in atlas creation by registration also used one of the subjects as representative image to which all others were registered. Nowadays the benefit of avoiding this bias is known and atlases are generated for an interpolated state from a group of images. Important concepts for realistic interpolation between images from spatial transformations

are geodesic rather than linear averaging for large deformations and ensuring that transformations are diffeomorphic [12]. Unfortunately enforcing the latter will introduce errors when registering whole abdominal images due to discontinuities at sliding boundaries. Furthermore our problem requires extrapolation and generation of unusual images, which is much harder than interpolation. We will employ dimensionality reduction and linear functions for regularization to avoid over-fitting and hence badly predictive models.

2 Material

MR images of the abdomen during free-breathing were acquired for 10 healthy volunteers according to the method proposed by von Siebenthal et al. [3]. These consisted of a sequence of interleaved 2D sagittal navigator and data slices, where the navigator slice is positioned in the center of the right liver lobe and the sagittal data slices cover the whole abdomen. The 2D images were acquired on a Philips Achieva 1.5T whole body MR system with a balanced turbo field echo sequence, a flip angle of 70^o, a TR=2.3ms, an in-plane resolution of 1.3x1.3mm^2, a slice thickness of 5mm and a temporal resolution of 163-226ms. To cover the abdomen, 53-65 data slices with a size of 224×224-240×240 pixels were required. To simulate short 4D-MRIs, only the first K=30 observations per data slice were processed, which would require a total acquisition time of 9-12min.

3 Method

The inter-leaved MR sequences, used for reconstructing the 4D-MRIs, consist of alternating acquisitions of a navigator slice N at the same liver position and a data slice D^a at changing positions $a = 1, ..., A$ to cover the whole abdomen, see Fig. 1. The problem of 4D reconstruction is to find for a given data slice D^a the remaining data slices $D^{b \neq a}$ which show the same liver motion state.

Selection Methods. So far, this problem has been approached by selecting data slices which are enclosed by most similar navigator images [3, 4]. The selection criteria has been based on the similarity of either the liver motion [3] or the image intensities [4] of the navigators.

In the former approach [3], the 2D navigator images were registered to a reference navigator image within the liver region using a B-Spline based registration method [13]. Then for each navigator image (N_i), the 2D displacement vectors at the C control points which lie within the liver ($\mathbf{u}_{c,i}^T = [u_{1,c,i}\ u_{2,c,i}]$ for $c = 1, 2...C$) are extracted. Finally for data slice D_i^a, with enclosing navigator images (N_i, N_{i+1}), D_j^b (with enclosing navigators (N_j, N_{j+1})) is selected for slice position b if it minimizes the overall dissimilarity measure $d_{i,j}^u$, i.e. $\arg\min_j d_{i,j}^u = \frac{1}{C} \sum_{c=1}^{C} |\bar{\mathbf{u}}_{c,i} - \bar{\mathbf{u}}_{c,j}|_2$, where $\bar{\mathbf{u}}_{c,i} = (\mathbf{u}_{c,i} + \mathbf{u}_{c,i+1})/2$. We also tested the selection performance after dimensionality reduction of the $K \times 2C$ dimensional dissimilarity matrix $\mathbf{M}^{u,i}$, which is given by $\mathbf{M}_{j,c}^{u,i} = \bar{u}_{1,c,i} - \bar{u}_{1,c,j}$ and

$\mathbf{M}^{u,i}_{j,C+c} = \bar{u}_{2,c,i} - \bar{u}_{2,c,j}$ for $c = 1, 2...C$ and $j = 1, 2, ...K$. Using Principle Component Analysis (PCA), Laplacian Eigenmaps or Neighbourhood Preserving Embedding (NPE), dissimilarity matrix $\mathbf{M}^{u,i}$ was transformed to a $K \times L$ dimensional matrix $\tilde{\mathbf{M}}^{u,i}$ and the optimal D^b_j determined by $\arg\min_j \tilde{d}^u_{i,j} = \frac{1}{L}\sum_{l=1}^{L} |\tilde{\mathbf{M}}^{u,i}_{j,l}|_2$.

In the intensity-based approach [4], each navigator image was first normalized to have an intensity distribution with zero mean and unit standard deviation. The $K \times R$ dissimilarity matrix $\mathbf{M}^{N,i}$ was then defined by $\mathbf{M}^{N,i}_{j,r} = N_{r,i} - N_{r,j}$ for $r = 1, 2, ...R$ and $j = 1, 2, ...K$, where $N_{r,i}$ is the normalized intensity of navigator N_i at pixel r. Laplacian Eigenmaps were used for dimensionality reduction of $\mathbf{M}^{N,i}$ to a L=3 dimensional manifold. The data slice with the smallest Euclidean distance in this 3D space ($\arg\min_j \tilde{d}^N_{i,j} = \frac{1}{L}\sum_{l=1}^{L} |\tilde{\mathbf{M}}^{N,i}_{j,l}|_2$) was then selected.

Prediction Methods. We propose to actively predict data slices instead of only selecting from the pool of available data slices. The aim is to predict the motion required to warp an existing data slice (D^b_j) to a similar liver position as the observed data slice (D^a_i) from the dissimilarity of the associated navigators ($\mathbf{M}^{u,i}$ or $\mathbf{M}^{N,i}$ denoted as $\mathbf{M}^i$). Our approach consists of the following steps:

- Pre-processing
  - (S1) Determine dissimilarity $\mathbf{M}^i$ for all navigator images
  - (S2) Determine data-slice displacement fields ($\mathbf{V}^j$) by registering all K data slices from the same position to each other
  - (S3) Dimensionality reduction of $\mathbf{M}^i$ and $\mathbf{V}^j$
- For each data slice D^a_i, with enclosing navigator images (N_i, N_{i+1}), and for all slice positions $b = 1...B$
  - (S4) Select most similar data slices D^b_j based on minimizing $\tilde{d}^{\mathbf{u}}_{i,j}$ (or $\tilde{d}^N_{i,j}$)
  - (S5) Determine linear function parameters $\mathbf{Q}$ from $\tilde{\mathbf{M}}^i$ and $\tilde{\mathbf{V}}^j$
  - (S6) Predict D^b_j motion from zero dissimilarity ($\mathbf{M}^i_{j,c}$=0 $\forall$ c) and $\mathbf{Q}$

For step S1, the dissimilarity between navigators ($\mathbf{M}^{u,i}$ or $\mathbf{M}^{N,i}$) was determined in the same way as for the selection method.

For registering the data slices (step S2) we used the deeds registration method [14, 15], as we want to register the whole images and it is currently one of the most accurate methods for registering images with sliding boundaries. Furthermore it is fast (≈0.5s per slice) and publically available. It was configured to provide displacement vectors at every 4th pixel in the image. We denote the displacement field from registering D^b_j to D^b_k by $\mathbf{v}^T_{j,k}$=[$v_{1,1,j,k}$ ... $v_{1,P,j,k}$ $v_{2,1,j,k}$ ... $v_{2,P,j,k}$], with P=R/16. Including zero displacements for $\mathbf{v}^T_{j,j}$ and collecting all results for D^b_j in $\mathbf{V}^j = [\mathbf{v}_{j,1}...\mathbf{v}_{j,K}]^T$ provides a $K \times 2P$ matrix.

Dimensionality reduction methods were applied in step S3 to $\mathbf{M}^{u,i}$ (or $\mathbf{M}^{N,i}$) and $\mathbf{V}^j$ to avoid underdetermined systems in step S5. The low-dimensional projections are denoted as $\tilde{\mathbf{M}}^i$ and $\tilde{\mathbf{V}}^j$, with dimensions $2C$ (or R) and $2P$ being reduced to $L_{\mathbf{m}}$ and $L_{\mathbf{v}}$ respectively. We used $L_{\mathbf{m}}$=$L_{\mathbf{v}}$=3 and employed PCA or NPE as these allow, in contrast to Laplacian Eigenmaps, construction of the full displacement field in step S6.

During the reconstruction, we first selected in step S4 the most similar data slice D_j^b by one of the previously described selection methods.

In step S5, the system of linear equations $\tilde{\mathbf{V}}^j = [\tilde{\mathbf{M}}^i \ \mathbf{1}]\mathbf{Q}$ was then solved in the least squares sense for the $(L_\mathbf{m} + 1) \times L_\mathbf{v}$ parameter matrix $\mathbf{Q}$.

In the final step (S6), we want to determine motion $\mathbf{v}_{j,i}$ such that the resulting transformed image ($\check{D}_j^b$) should have the liver in a similar motion state as data slice D_i^a. So far we have learned how the dissimilarity in navigators ($\tilde{\mathbf{M}}^i$) relate to motion between data slices ($\tilde{\mathbf{V}}^j$). This learned function is now used to predict the required data slice motion for the given navigator pair, i.e. for a zero dissimilarity. In details, motion $\tilde{\mathbf{v}}_{j,i}$ was predicted by $\tilde{\mathbf{v}}_{j,i}^T = [\tilde{\mathbf{z}}^T \ 1]\mathbf{Q}$, where $\tilde{\mathbf{z}}$ is the L_m dimensional zero vector mapped to the low-dimensional space. The predicted motion $\tilde{\mathbf{v}}_{j,i}$ was then mapped back to the high-dimensional ($2P$) space and applied to data slice D_j^b to get $\check{D}_j^b$.

To improve SNR, steps S4 to S6 were performed for the T=5 most similar data slices and the resulting transformed images were averaged to $\bar{D}^b$. Finally the 3D image, associated with data slice D_i^a, was formed by stacking the mean images $\bar{D}^b$ for $b = 1, ..., B$.

4 Results

Quantitative evaluation was performed by leaving out a data slice (which serves as ground truth (GT)), predicting it from the other available data slices and measuring the mean residual motion within the liver between the predicted and the GT data slice by image registration (deeds method [14, 15]). In this way the impact of the reconstruction errors on extracting the liver motion from 4D-MRIs can be measured. We evaluated the mean residual motion per subject for 25 liver slices and 30 temporal samples, and summarized this distribution by its mean and 95th percentile. We also assess the performance at the end-inhalation state and for the most unusual data slices. The latter were selected based on the GT data slice having navigators with a mean displacement difference ($d_{i,j}^u$) of 3mm or more to all other navigators for this slice.

Fig. 2 shows an example where the GT image is very dissimilar to the available data slices according to the corresponding navigator motion (Fig. 2b, $d_{i,j}^u$=4.2mm). Selecting the 5 most similar data slices leads not only to a blurry reconstruction but also to a misaligned liver (Fig. 2c). The prediction method is able to estimate most of this unseen motion (Fig. 2d).

Table 1 shows that higher accuracies were achieved when using the displacement information of the navigators rather than their intensities. PCA performed well against the other tested dimensionality reduction methods. Highest accuracies were achieved with predictions from navigator displacements and PCA, which provided a substantial mean improvement over the best selection method for end-inhalation states (23%) and for unusual positions (40%).

A coronal slice from a reconstruction example is shown in Fig. 3. An improved consistency across slices can be observed at the diaphragm, and for lung and liver vessels for the prediction method (Fig. 3b).

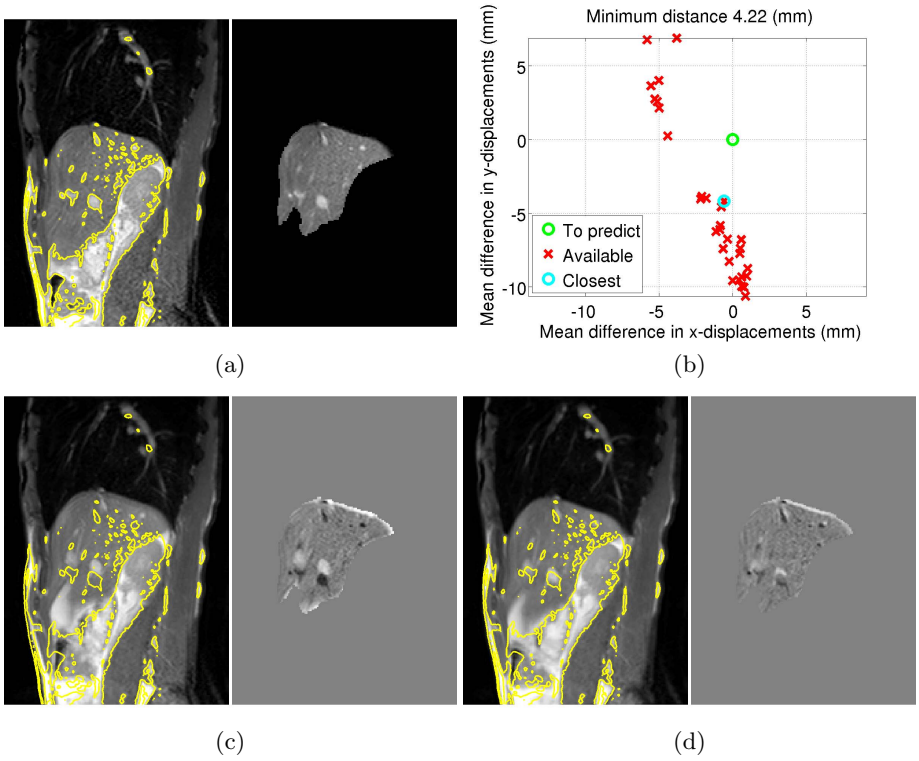

Fig. 2. (a) Ground-truth (GT) image (right: liver region) to predict, (b) 2D dissimilarity of available data slices (red crosses) to GT (green circle) based on difference in navigator displacements, (c,d) reconstructed slice (right: its difference to GT within liver) based on (c) selecting the 5 closest observations (meanError: 8.1mm), or (d) predicting the motion of 5 data slices from the navigator displacements after dimensionality reduction by PCA (meanError: 2.4mm). All yellow contours are from GT.

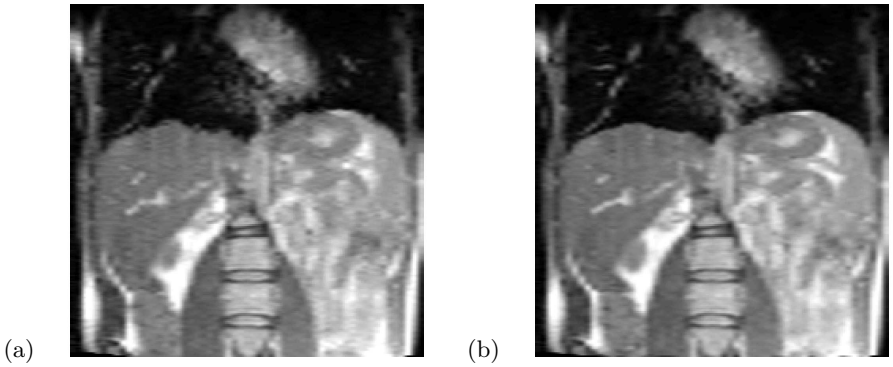

Fig. 3. Example of 3D reconstruction from 30 observations for (a) baseline selection method [3] and (b) proposed prediction method (navigator displacements, PCA)

Table 1. Mean performance results for 10 volunteers (in mm) for (a) all, (b) end-inhalation (10.8%) and (c) most unusual ($d^u_{i,j} \geq 3$mm, 16.4%) data slices when (Sel) selecting or (Pred) predicting the closest T=5 data slices from navigator (right) displacements or (left) intensities. Rows show results for dimensionality reduction methods. Best results are marked in bold. The baseline approach [3] is underlined.

	Mean Error											
	(a) All slices				(b) End-inhalation				(c) Most unusual			
	Displacement		Intensity		Displacement		Intensity		Displacement		Intensity	
DimRed	Sel	Pred	Sel	Pred	Sel	Pred	Sel	Pred	Sel	Pred	Sel	Pred
None	<u>0.93</u>	0.87	1.17		<u>1.28</u>	1.15	1.56		<u>2.16</u>	1.79	2.43	
PCA	0.94	**0.80**	1.19	1.43	1.28	**0.98**	1.55	1.87	2.17	**1.30**	2.43	2.52
Laplacian	1.54	n/a	2.53	n/a	2.24	n/a	3.32	n/a	2.92	n/a	4.11	n/a
NPE	1.11	1.91	2.43	2.53	1.54	2.15	3.17	3.41	2.36	2.83	3.96	4.32
	95% Error											
	(a) All slices				(b) End-inhalation				(b) Most unusual			
	Displacement		Intensity		Displacement		Intensity		Displacement		Intensity	
DimRed	Sel	Pred	Sel	Pred	Sel	Pred	Sel	Pred	Sel	Pred	Sel	Pred
None	<u>1.94</u>	1.79	2.71		<u>3.26</u>	2.76	3.70		<u>4.61</u>	4.08	4.84	
PCA	1.96	**1.57**	2.71	3.02	3.26	**2.02**	3.65	4.13	4.60	**2.99**	4.70	5.17
Laplacian	4.33	n/a	5.85	n/a	6.34	n/a	7.19	n/a	6.96	n/a	7.72	n/a
NPE	2.71	3.82	5.38	5.60	4.16	4.74	6.75	7.35	4.92	6.07	7.50	8.07

5 Discussion and Conclusion

We proposed a method for improving 4D-MRI reconstruction of rare motion states, by actively predicting the unseen motion rather than only selecting from the available data. The method is based on learning the relationship between the motion of the navigator images and the motion of the data slices by linear regression after dimensionality reduction. It is most powerful for unusual motion states where a 40% improvement in mean accuracy can be achieved. Where enough similar samples are available it is less needed, but also does no harm as it is well constrained.

Using navigator intensities rather than displacements was clearly inferior. Initial test with extrapolations showed that non-linear functions or high-dimensional spaces leading to high errors due to the limited number of samples.

Currently every data slice prediction is optimized independently, without considering the gathered information across slices or over time. Such a combined framework would certainly benefit to make the predictions more robust, as currently improvements for extreme motion states can be of different quality and hence reduce the data slice consistency despite being more accurate on average.

We envision that the proposed prediction method is used for the unusual but very important motion states, while the selection method, which is faster, is sufficient for the common states.

References

1. Tanner, C., Boye, D., Samei, G., Székely, G.: Review on 4D models for organ motion compensation. Critical Reviews in Biomedical Engineering 40(2), 135–154 (2012)
2. McClelland, J.R., Hawkes, D.J., Schaeffter, T., King, A.P.: Respiratory motion models: A review. Medical Image Analysis 17(1), 19–42 (2013)
3. Von Siebenthal, M., Székely, G., Gamper, U., Boesiger, P., Lomax, A., Cattin, P.: 4D MR imaging of respiratory organ motion and its variability. Phys. Med. Biol. 52, 1547 (2007)
4. Wachinger, C., Yigitsoy, M., Rijkhorst, E.J., Navab, N.: Manifold learning for image-based breathing gating in ultrasound and MRI. Medical Image Analysis 16(4), 806–818 (2012)
5. Tryggestad, E., Flammang, A., Han-Oh, S., Hales, R., Herman, J., McNutt, T., Roland, T., Shea, S.M., Wong, J.: Respiration-based sorting of dynamic MRI to derive representative 4D-MRI for radiotherapy planning. Medical Physics 40(5), 051909 (2013)
6. Baumgartner, C.F., Kolbitsch, C., McClelland, J.R., Rueckert, D., King, A.P.: Groupwise simultaneous manifold alignment for high-resolution dynamic MR imaging of respiratory motion. In: Gee, J.C., Joshi, S., Pohl, K.M., Wells, W.M., Zöllei, L. (eds.) IPMI 2013. LNCS, vol. 7917, pp. 232–243. Springer, Heidelberg (2013)
7. Fransens, R., Strecha, C., Van Gool, L.: Optical flow based super-resolution: A probabilistic approach. Computer Vision and Image Understanding 106(1), 106–115 (2007)
8. Wu, G., Wang, Q., Lian, J., Shen, D.: Estimating the 4D respiratory lung motion by spatiotemporal registration and building super-resolution image. In: Fichtinger, G., Martel, A., Peters, T. (eds.) MICCAI 2011, Part I. LNCS, vol. 6891, pp. 532–539. Springer, Heidelberg (2011)
9. Hamm, J., Ye, D.H., Verma, R., Davatzikos, C.: Gram: A framework for geodesic registration on anatomical manifolds. Medical Image Analysis 14(5), 633–642 (2010)
10. Gerber, S., Tasdizen, T., Fletcher, T., Joshi, S., Whitaker, R.: Manifold modeling for brain population analysis. Medical Image Analysis 14(5), 643–653 (2010)
11. Wu, G., Jia, H., Wang, Q., Shen, D.: Sharpmean: Groupwise registration guided by sharp mean image and tree-based registration. NeuroImage 56(4), 1968–1981 (2011)
12. Avants, B., Gee, J.C.: Geodesic estimation for large deformation anatomical shape averaging and interpolation. Neuroimage 23, S139–S150 (2004)
13. Hartkens, T., Rueckert, D., Schnabel, J.A., Hawkes, D.J., Hill, D.L.G.: VTK CISG registration toolkit: An open source software package for affine and non-rigid registration of single-and multimodal 3D images. In: Bildverarbeitung für die Medizin 2002, pp. 409–412 (2002)
14. Heinrich, M.P., Jenkinson, M., Brady, S.M., Schnabel, J.A.: Globally optimal deformable registration on a minimum spanning tree using dense displacement sampling. In: Ayache, N., Delingette, H., Golland, P., Mori, K. (eds.) MICCAI 2012, Part III. LNCS, vol. 7512, pp. 115–122. Springer, Heidelberg (2012)
15. Heinrich, M., Jenkinson, M., Brady, M., Schnabel, J.A.: MRF-based deformable registration and ventilation estimation of lung CT. IEEE Transactions on Medical Imaging 32(7), 1239–1248 (2013)